AGU PUBLICATIONS

JGR

Journal of Geophysical Research: Oceans

RESEARCH ARTICLE

10.1002/2017JC012798

Assessing variability in the size and strength of the North Atlantic subpolar gyre

Nicholas P. Foukal[1] **and M. Susan Lozier**[1]

[1]Division of Earth and Ocean Sciences, Nicholas School of the Environment, Duke University, Durham, North Carolina, USA

Key Points:
- A new index of variability in the size and strength of the gyre is derived from satellite altimetry (1993–2015)
- The gyre's strength is declining more slowly than previously estimated and no decline is detected in the gyre's size
- Zonal movements of the gyre's eastern boundary are generally small and not correlated to the properties in the eastern subpolar gyre

Correspondence to:
N. P. Foukal,
Nicholas.Foukal@Duke.edu

Citation:
Foukal, N. P., and M. Susan Lozier (2017), Assessing variability in the size and strength of the North Atlantic subpolar gyre, *J. Geophys. Res. Oceans*, *122*, 6295–6308, doi:10.1002/2017JC012798.

Received 14 FEB 2017
Accepted 6 JUL 2017
Accepted article online 11 JUL 2017
Published online 14 AUG 2017

Abstract Recent studies on the size and strength of the North Atlantic subpolar gyre (SPG) offer contrasting assessments of the gyre's temporal variability: studies that use empirical orthogonal function (EOF) analyses of satellite sea-surface height (SSH) report a rapid decline in SPG size and strength since 1992 (~20% per decade), while concurrent in situ observations report either no trend or a slight decline. Here we investigate this discrepancy by analyzing the size and strength of the SPG with satellite SSH from 1993 to 2015 with two separate methods: indirectly via EOF analysis and more directly through measurements of the gyre center and boundary. We define the boundary of the gyre as the largest closed contour of SSH, the center as the minimum SSH, and the strength as the difference between the SSH at the boundary and the center. We identify a linear decline over the study period in the SPG strength (5.1% per decade), but find no statistically significant trend in the SPG area. The trend in the gyre strength is weaker than the EOF-based trend and is most likely below the level of detection of the in situ measurements. We conclude that the variability previously identified as a sharp decline in SPG circulation can be more appropriately attributed to basin-wide sea level rise during the satellite altimetry period. In addition, we find that the properties of the eastern SPG do not covary with the SPG size, suggesting that SPG dynamics do not control the strength of the intergyre throughput.

Plain Language Summary For over a decade there has been a discrepancy in the observed variability of the size and strength of the subpolar gyre: satellite estimates based on the height of the sea-surface were interpreted as showing a rapid decline in the gyre since the early 1990s, while direct measurements from ships and moorings showed the gyre to be quite stable over the same time period. In this work, we reconcile these two measurement techniques by subtracting the long-term sea level rise from the satellite altimetry. Changes to ocean circulation require changes to the slope of the sea-surface, so sea-surface height variability that is present across the gyre can obscure variability in the ocean circulation. Our new measures of the size and strength of the gyre indicate a weakening, but at about 1/4 the rate of previous estimates, and a stable gyre size over the study period. Both of these are consistent with the direct measurements. In addition, we find that the eastern boundary of the gyre does not have large coherent excursions to the east and west, and we find that it most likely does not control the temperature and salinity the eastern subpolar region as has been previously theorized.

1. Introduction

Wind-driven Ekman divergence in the subpolar North Atlantic leads to a bowl-shaped mean sea-surface height (SSH) field (Figure 1a), which in turn drives a cyclonic geostrophic subpolar gyre (SPG) around a minimum SSH. The size and strength of this gyre have been theorized to affect the amount of throughput from the subtropical gyre (STG) to the SPG, which is essentially the upper limb of the Atlantic Meridional Overturning Circulation (AMOC) at intergyre latitudes [*Bersch*, 2002; *Häkkinen and Rhines*, 2004, 2009; *Hátún et al*., 2005; *Holliday*, 2003; *Zhang*, 2008]. According to this hypothesis, when the eastern boundary of the SPG contracts westward, more water from the STG penetrates northward, warming the SPG [*Häkkinen et al*., 2013]; an eastward expansion brings a contrasting result.

To track the size and strength of the SPG, *Häkkinen and Rhines* [2004] and *Hátún et al*. [2005] use empirical orthogonal function (EOF) analyses of SSH across the North Atlantic. They interpret the leading mode (termed the "Gyre Index") as a metric of the gyre's size [*Hátún et al*., 2005] and strength [*Häkkinen and*

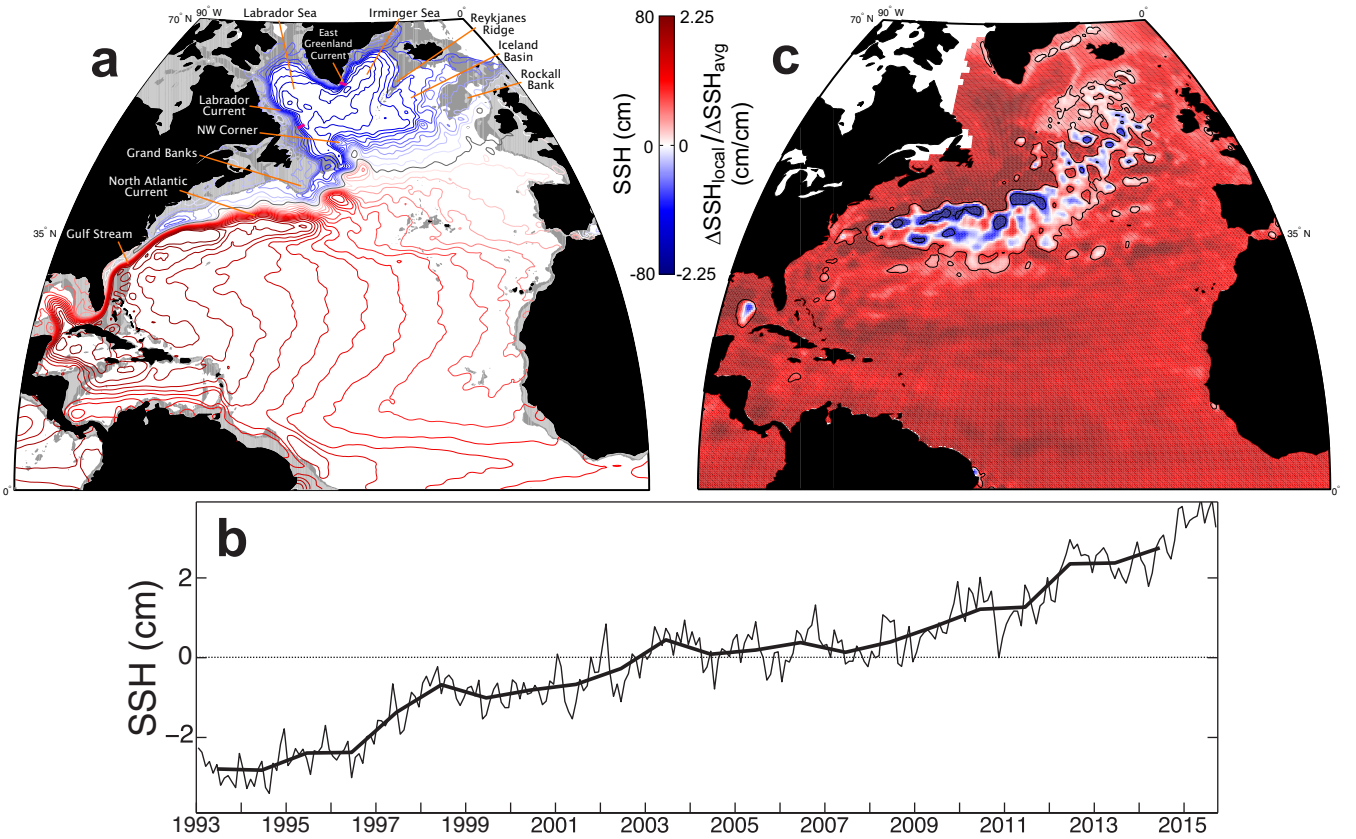

Figure 1. Temporal and spatial averages of North Atlantic SSH. (a) Time-mean SSH depicting the SPG bowl and STG dome with locations of interest shown. Zero SSH contour shown in gray and contour interval is 5 cm. Magenta lines in the Labrador and East Greenland currents depict the approximate locations of the 53°N and OVIDE lines. (b) Time series of North Atlantic basin-averaged SSH (0°N–70°N, 90°W–0°W) from 1993 to 2015 (monthly = thin line, annual = thick line). (c) Linear slopes of local SSH regressed onto the basin-averaged SSH time series. Stippling denotes statistically significant ($p < 0.05$) correlations, covering most of the study area.

Rhines, 2004]. As formulated, the Gyre Index indicates that the SPG contracted and the Labrador Current (at the SPG western boundary) weakened by 7–10 Sverdrups (Sv.; 1 Sv. = 10^6 m^3 s^{-1}; 18–25% decline) from 1992 to 2002 [*Häkkinen and Rhines*, 2004]. Since 2002, the Gyre Index has continued to decline with reported impacts on the nutrient supply to the SPG [*Johnson et al.*, 2013] as well as on the SPG temperature and salinity due to increased transport from the STG [*Häkkinen and Rhines*, 2004; *Hátún et al.*, 2005; *Sarafanov et al.*, 2008; *Zhang*, 2008; *Häkkinen and Rhines*, 2009; *Sherwin et al.*, 2012; *Häkkinen et al.*, 2013]. To validate their interpretation of the Gyre Index as a metric of SPG strength, *Häkkinen and Rhines* [2004] point to declining current velocities at a mooring in the western Labrador Sea over the 19 month period between October 1996 and April 1998.

In contrast, in situ observations of the SPG circulation covering longer time periods and larger spatial scales do not depict a strongly declining gyre. Results from a mooring array at 53°N from 1997 to 2010 in the Labrador Current reveal a warming, but no trend in current velocities between 200 and 2800 m [*Fischer et al.*, 2010; *Xu et al.*, 2013]. Furthermore, while a combination of satellite altimetry and WOCE AR7W hydrographic transects from 1993 to 2004 shows a declining Labrador Current in the 1990s, these same records show a rebound in the early 2000s [*Han et al.*, 2010], in agreement with results from a multimodel study on SPG circulation strength [*Böning et al.*, 2006]. A more recent study analyzing the middepth (1000 m) circulation pattern over the entire SPG from PALACE and ARGO profiling floats in three periods (1997–2001, 2002–2006, and 2006–2010) concludes that while the SPG weakened in the middle period it mostly recovered in the third period, such that over the entire 12 years there was only a slight linear decline (8% per decade) in the current speeds [*Palter et al.*, 2016]. Finally, a reconstruction of the East Greenland Current, using a combination of satellite altimetry from 1992 to 2009, moorings from 2004 to 2006 and repeat hydrography of the OVIDE line between 1994 and 2008, shows a stable boundary current with no long-term trend [*Daniault et al.*, 2011].

These conflicting estimates of long-term variability in SPG strength have motivated a closer inspection of the Gyre Index. This inspection has identified several potential issues with its interpretation as an index of SPG circulation. Most prominently, basin-wide sea level rise over the study period [e.g., *Cazenave and Llovel*, 2010; *Church et al*., 2013] may be affecting the ability of the Gyre Index to isolate SPG circulation signals, which require a change in the SSH gradient field, from variability that is present across the basin. Another potential issue is the definition of the Gyre Index as the leading mode of SSH across the entire North Atlantic basin (0°N–70°N, 90°W–0°W: note that sometimes 15°N is used as the southern boundary). With this definition, variability in SSH across the entire North Atlantic—not just the SPG—determines the Gyre Index. A third concern is that the weighting of this leading mode in the eastern SPG (50°N–58°N, 35°W–18°W), where the expansion/contraction of the SPG is hypothesized to control the amount of STG water that reaches the SPG, is weak. Thus, variability in the eastern SPG is not strongly reflected in the Gyre Index, yet the Gyre Index is primarily used to explain variability in that region. Finally, though the Gyre Index is hypothesized to track both the size and strength of the SPG, it is not immediately clear that these two variables covary nor whether the leading mode of SSH is more related to one or the other.

The overall objective of this study is to reconcile the conflicting views of the temporal variability of the SPG strength and to address the abovementioned questions about the Gyre Index. The specific goals are to: (1) formulate a more direct measurement of the SPG area and strength, (2) use those measurements to assess the validity of the Gyre Index as a metric of SPG area and strength, (3) determine the seasonal, interannual, and long-term variability of the SPG size and strength, and (4) investigate possible forcing mechanisms for this variability.

2. Data and Methods

We estimate the size and strength of the SPG with two separate methods: (1) indirectly through two EOF analyses of the North Atlantic SSH (sections 3.1 and 3.3, along the lines of *Häkkinen and Rhines* [2004], *Hátún et al*. [2005], *Häkkinen and Rhines* [2009], and *Häkkinen et al*. [2013]) and (2) more directly by measuring the SPG center and boundary as a function of time (section 3.2).

For both methods, we start with gridded $1/4°$ AVISO absolute dynamic topography (ADT) fields in the North Atlantic (0°N–70°N, 90°W–0°W) at daily resolution from January 1993 to September 2015 [http://www.aviso.altimetry.fr/duacs/]. ADT is a measure of the local deviation from the geoid. For simplicity, we refer to the ADT fields as SSH in the remainder of the text. The SSH data are then averaged into monthly means to analyze longer time scales.

For both EOF analyses, the local monthly climatology is removed and the SSH data are binned to 1° spatial resolution to focus on large-scale dynamics as well as to retain consistency with previous derivations of the Gyre Index [e.g., *Häkkinen and Rhines*, 2004]. To analyze modes of variability beyond the linear trend, we perform a second EOF analysis with SSH data that are detrended by subtracting the basin-averaged time series, and then normalized by the local standard deviation to yield a data set of SSH with zero mean, unit variance, and no trend. Normalization to unit variance gives each location equal weighting in the EOF analysis rather than providing more weight to locations with higher variance [*Manly*, 2005].

To ensure that we are capturing the same variability in the Gyre Index as in previous derivations, we compare our index (from our first EOF analysis) to those reported in *Häkkinen and Rhines* [2004], *Zhang* [2008], *Häkkinen et al*. [2013], and *Han et al*. [2014]. Our Gyre Index has similar spatial weightings and time series as previous derivations from shorter periods, but only captures 9.1% of the total variance, compared to 11.1% (1993–2002) [*Häkkinen and Rhines*, 2004], 30% (1993–2003 with annual resolution) [*Zhang*, 2008], 20.3% (1993–2012) [*Häkkinen et al*., 2013], and 14% (1992–2012) [*Han et al*., 2014] reported from previous studies. If the SSH data from 1993 to 2015 are normalized prior to passing into the EOF analysis, the spatial pattern and time series of the leading mode are nearly identical to those of the non-normalized data, but the variance explained increases to 25.0% (not shown). If we limit the EOF to 1993–2002, we recover a Gyre Index almost identical to that reported in *Häkkinen and Rhines* [2004]: it explains 11.5% of the variance, weights negatively over most of the study area, and its principal component (PC) has a statistically significant trend of -1.58 cm yr^{-1}. Overall, we find that the leading mode of North Atlantic SSH from 1993 to 2015 is largely similar to the Gyre Index derived with the first decade of SSH (1993–2002), but by extending the time period to 2015, the variance explained by this mode decreases slightly from 11.1% to 9.1%.

To measure the size and strength of the SPG directly, we return to the monthly, 1/4° SSH data set. We define the gyre boundary as the largest closed contour of each monthly SSH field, with 1 cm intervals for the contours. We define the gyre center as the minimum SSH that is both within the gyre boundary and north of 53°N. This latter constraint eliminates the possibility of the gyre center occurring inside strong cyclonic eddies near the SPG's southern boundary, where the North Atlantic Current (NAC) retroflects around the Northwest Corner and sheds both cyclonic and anticyclonic eddies. We define the gyre area as the surface area enclosed by the gyre boundary and we consider the difference between the SSH at the boundary and at the center an index of the gyre strength. This metric of the gyre strength is based on the local sea-surface slope setting the local barotropic flow. When this relationship is horizontally integrated between the gyre center and boundary to calculate the gyre transport, the local sea-surface slope simplifies to $\Delta(SSH)$, or the difference in elevation between the gyre center and boundary. Thus, the gyre transport due to the barotropic flow field is linearly related to the depth of the SSH bowl in the SPG. Finally, a limitation of our measure of gyre strength is that it does not account for the baroclinic mode of the gyre, however the dominance of the barotropic mode in the thermocline waters (<1000 m depth) of the SPG has been well-documented [e.g., *Häkkinen and Rhines*, 2004; *Sarafanov et al.*, 2012; *Daniault et al.*, 2011; *Zantopp et al.*, 2017].

Long-term trends in the time series and their p values are calculated using Sen's slope with deseasonalized monthly data to reduce autocorrelation in the time series and to eliminate the potential for seasonal biasing by starting our analysis in January (of 1993) and ending in September (of 2015). All trends and correlations reported here exceed the 95% statistical significance threshold ($p < 0.05$) unless otherwise noted.

Winter North Atlantic wind stress curl (WSC) is calculated from NCEP/NCAR Reanalysis wind vectors [*Kalnay et al.*, 1996] and averaged from December through March. The EOF analysis of WSC (Figure 6) covers the spatial range 22°N–68°N, 83°W–7°W. The data were neither detrended nor normalized to the local variances so as to mimic the initial EOF analysis of SSH (described above), thus facilitating a direct comparison.

The NAO time series is the winter (DJFM) NAO index from the NCAR/UCAR Climate Data Guide [*Hurrell and National Center for Atmospheric Research Staff*, 2016]. The East Atlantic (EA) pattern time series is averaged over the winter (DJFM) months from the monthly EA time series acquired from the NOAA Climate Prediction Center. In Figure 5d, the time series of salinity in the eastern SPG (53°N–62°N, 25°W–12°W, 0–500 m) is extracted from gridded, monthly EN4 (version EN.4.1.1) data [*Good et al.*, 2013].

3. Results and Discussion

3.1. EOF Analysis of North Atlantic SSH

3.1.1. Evidence for the Gyre Index Reflecting Basin-Scale Sea Level Rise

To determine the extent to which the Gyre Index reflects North Atlantic sea level rise, we first investigate the mean SSH time series and its spatial signature in the North Atlantic (Figures 1b and 1c). When averaged over the spatial domain (0°N–70°N, 90°W–0°W), the basin-averaged SSH has increased steadily over the study period (0.21 cm yr^{-1}). This rise exhibits a nearly basin-wide pattern: a linear regression of the local SSH onto the basin-averaged SSH (Figure 1c) yields statistically significant positive slopes over 90% of the study area.

A comparison of the Gyre Index's spatial pattern (Figure 2a) to the spatial variability in the observed sea level rise (Figure 1c) demonstrates that the two are largely mirror images of each other—strong weights in the central Labrador and Irminger Seas, inshore and north of the Gulf Stream/North Atlantic Current (GS/NAC), and opposite weights south of the GS/NAC. The opposing sign between the two figures is irrelevant because the sign convention in an EOF analysis is arbitrary. In addition, the time series of the Gyre Index (Figure 2b) is strongly negatively correlated to the basin-averaged SSH time series ($r_{monthly} = -0.99$, $r_{annual} = -1.00$). In the Gyre Index, a declining trend (-0.88 cm yr^{-1}, Figure 2b) and negative weights across 96% of the study area (basin mean of Figure 2a $= -0.21$, unitless) are consistent with increasing SSH over the study period, as seen in Figures 1b and 1c. Thus, these results indicate that the Gyre Index is largely capturing the SSH variability arising from basin-wide sea level rise across the North Atlantic.

This strong correlation between the Gyre Index and North Atlantic SSH indicates that the Gyre Index is isolating variability due to sea level rise rather than the dynamics within the basin. A uniform rise or fall of SSH

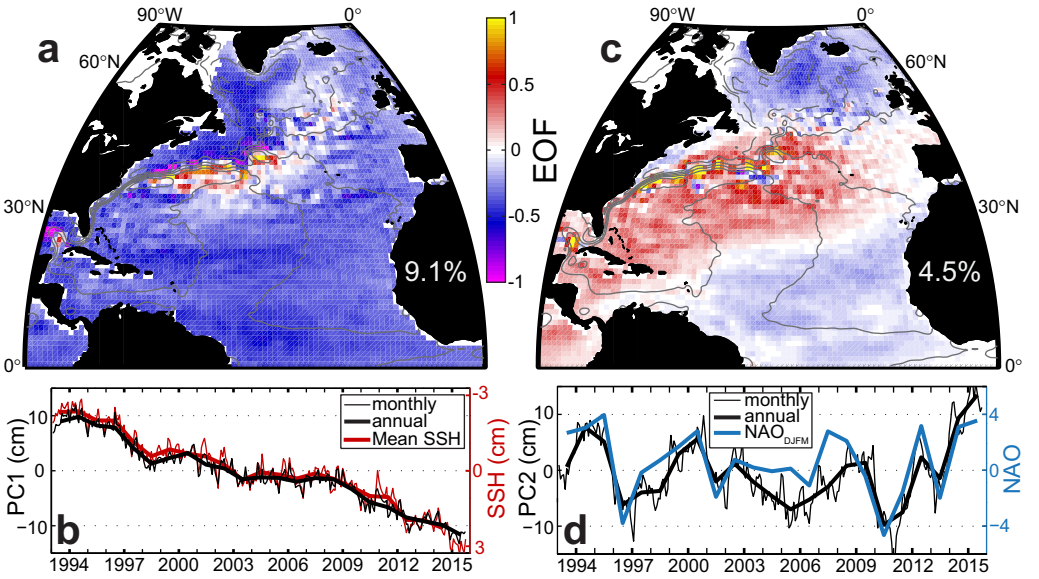

Figure 2. EOF analysis of nondetrended SSH. (a) EOF1 (9.1% of total variance) and (b) PC1 of North Atlantic SSH are defined to be the Gyre Index. Basin-averaged SSH (b, red, *y* axis inverted) is strongly correlated to the Gyre Index ($r_{annual}=-1.00$). (c) EOF2 (4.5% of total variance) captures the NAO tripole spatial pattern and (d) PC2 is correlated ($r = 0.78$) to the winter NAO (blue). Time-mean SSH contours are shown in gray in Figures 2a and 2c (dashed = negative).

is not a signature of dynamical variability, only spatial structure in the Gyre Index would indicate a dynamic response. A close inspection of Figure 2a does show some spatial structure, such as in the Labrador Sea where the central part of the basin has a more negative weighting than the boundary. This would indicate that the gyre center is rising faster than the boundary, thereby flattening the SPG bowl and weakening the gyre, as explained in *Häkkinen and Rhines* [2004]. However, because the central portions of the gyre and the edge of the gyre are both rising, one cannot infer the rate at which the SPG strength (a dynamical measure) is declining solely from the Gyre Index time series. Instead, one needs to consider the difference in sea level between the gyre center and boundary rather than basin-wide sea level change. Simply put, the basin-wide trend in sea level rise is masking changes in gyre dynamics. Thus, to isolate variability in gyre dynamics, the basin-wide SSH signal must be removed prior to EOF analyses, a calculation discussed in section 3.3.

3.1.2. Implications of the Gyre Index's Linkage to the Basin-Wide Sea Level Rise

Given that the Gyre Index does show some spatial structure, we examine whether this structure possibly reflects changes to the gyre size. Because the gyre is topographically constrained on its northern and western boundaries, variability of the gyre size is primarily due to changes in the location of its eastern and southern boundaries. However, there is almost no weighting of the Gyre Index (Figure 2a) to the west of Rockall Bank (mean from 50°N to 58°N, 35°W to 18°W = 0.12 ± 0.11 SD, unitless), where the eastern edge of the SPG lies [*Rypina et al.*, 2011], raising the question as to whether the Gyre Index is tracking the eastward expansion/contraction of the gyre. Conceptually, an expanded SPG would result in depressed SSH in the eastern SPG, while periods with a contracted SPG would show a SSH rise in the eastern SPG—so we would expect a negative weighting of this mode in the eastern SPG. Contrary to these expectations, the eastern SPG weights very weakly in the Gyre Index.

The Gyre Index has also been used to explain meridional shifts in the GS/NAC. The positive weightings of the Gyre Index (Figure 2a) to the south of the mean GS/NAC position (indicated by the closely spaced mean SSH contours in Figure 1a) led *Zhang* [2008] to infer that the GS/NAC has been consistently shifting southward over the satellite altimetry period. She connects this southward shift in the GS/NAC to a weakened SPG and a stronger AMOC, the latter indicated by increasing OHC at 400 m in the SPG. However, while a southward shift in the GS/NAC can explain the decreasing SSH south of the GS/NAC, the concurrent SSH rise north of the GS/NAC is not explained by this shift. We note that three indices of the meridional GS position from 1993 to 2012 do not have long-term trends [*Perez-Hernandez and Joyce*, 2014]. Thus, in the absence of in situ data indicating that the GS/NAC was shifting southward over this time period, there appears to be little evidence that the Gyre Index is tracking the meridional position of the GS/NAC—a

finding consistent with the suggestion that the Gyre Index is primarily reflecting the thermodynamic, and not the dynamic, variability of the North Atlantic.

3.1.3. The NAO Signature in North Atlantic SSH

The second mode of the SSH EOF reflects the familiar tripole NAO pattern which results from basin-scale wind variability (Figure 2c). The principal component (PC, Figure 2d) of this mode is correlated to the winter NAO ($r = 0.78$). Though this tripole pattern—in which the STG fluctuates out-of-phase with both the SPG and the tropical Atlantic—is more commonly expressed in SST [e.g., *Deser et al*., 2010], SSH variability shows a similar pattern. There are two mechanisms used to explain the opposing responses of the two gyres to the NAO: (1) Ekman forcing over the basin leads to immediate opposing signatures in the convergence of surface waters in the STG and SPG [e.g., *Marshall et al*., 2001; *Deshayes and Frankignoul*, 2008; *Lozier et al*., 2008; *Williams et al*., 2014] and (2) opposing surface buoyancy fluxes between the gyres on multiannual time scales leads to cooling in one gyre while the other is warming [e.g., *Deshayes and Frankignoul*, 2008]. NAO forcing was previously connected to the leading mode of TOPEX/POSEIDON SSH data from 1992 to 1998 [*Esselborn and Eden*, 2001]. During that time period, the strong shift in the NAO from the winter of 1995 to the winter of 1996 dominated SSH variability such that the NAO explained 34% of the total variance. Using the altimetry time series to 2015, this mode has diminished in importance, now explaining only 4.5% of the variance. Interestingly, though the NAO mode derived here is by definition orthogonal to the Gyre Index, both indices have been invoked as controlling mechanisms for the size of the SPG [e.g., *Hátún et al*., 2005]. This confusion provides further motivation for deriving an alternate index of the SPG size and strength.

3.2. Directly Measured SPG Area and Strength

3.2.1. Mean and Seasonality

We now analyze our more direct measure of SPG size and strength. We start by evaluating the mean of these variables and then turn to their variability on seasonal and then interannual time scales. The mean SPG boundary (Figure 3a) corresponds well with a stream function calculated from surface drifter trajectories [*Rypina et al*., 2011]. Classically, the definition of the SPG has encompassed the entire Iceland Basin up to, and sometimes across Rockall Bank [e.g., *Rossby*, 1996; *Lavender et al*., 2000; *Fratantoni*, 2001; *Curry and Mauritzen*, 2005; *Hátún et al*., 2005]. However, in the present definition of the SPG, with a focus on a closed contour, not all eastern subpolar waters fall within the SPG.

In the mean, the geographic area enclosed by the SPG boundary covers 2.68 * 10^6 km^2 ($\pm$0.24 * 10^6 km^2, SD) and the SPG strength is 35 $\pm$ 4 cm. Geographically, much of the seasonal variability is expressed in either the northeastward extent of the boundary toward Iceland or the southwestward extent around the

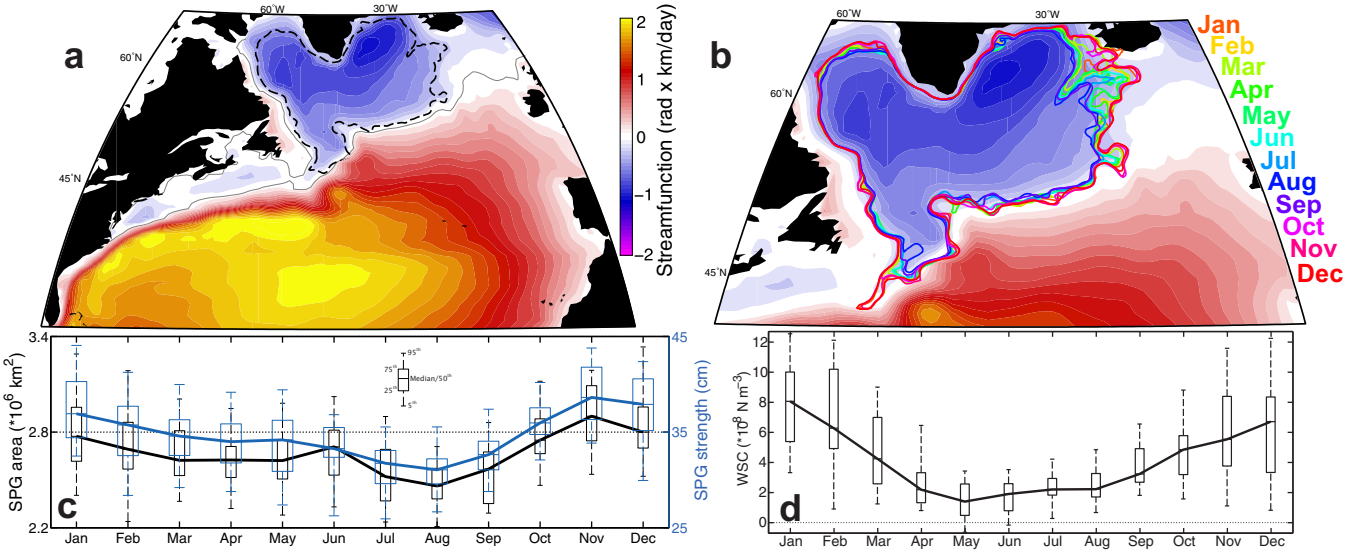

Figure 3. Mean and seasonality of SPG size and strength. (a) Mean SPG boundary (dashed) compared to the surface stream function calculated from surface drifters [*Rypina et al*., 2011]. (b) SPG boundaries in each climatological month. Month names are colored according to the color of their boundary. (c) Climatological monthly SPG area (black) and strength (blue, right *y* axis) are at a minimum in July to September and are highest from November to January ($r = 0.95$). (d) Climatological WSC over the SPG (50°N–68°N, 60°W–5°W) has similar seasonality.

Grand Banks (Figure 3b). The SPG boundary expands to its largest extent and the gyre becomes strongest in November and the gyre contracts to its smallest size and becomes weakest in August, confirming that the gyre size and strength covary on seasonal time scales (Figure 3c, $r_{seasonal} = 0.95$). We term these concurrent oscillations in the gyre size and strength "dilations": as the SPG enlarges, the SSH bowl deepens and when the SPG contracts, the SSH bowl flattens. The range of seasonal variability is roughly ±8% of the mean in both area and strength with higher variances occurring primarily in the winter months. This seasonality suggests a relatively fast spin-up of the gyre in the autumn due to the onset of strongly positive WSC forcing, and a more gradual slow-down in response to relaxed WSC forcing in the spring and summer months (Figure 3d).

3.2.2. Interannual Variability

On interannual time scales, the variability in the geographic area and strength of the SPG is on the same order as the seasonal variability (±10% of the mean). Also similar to the seasonal variability, large portions of the interannual variability in gyre area is expressed in the southwestward extent around the Grand Banks and in the northeastward extent toward Iceland (Figure 4a).

The time series of SPG size and strength from 1993 to 2015 (Figure 4b) show that the SPG dilates on interannual time scales at both monthly and annual resolution ($r(\text{area,strength})_{monthly} = 0.81$, $r(\text{area,strength})_{annual} = 0.68$). Large variability at monthly time scales in both variables is evident, as well as peaks/troughs spaced ~5 years apart: peaks in 1997, 2002, 2007, and 2014, and troughs in 1994, 2000, 2005, and 2010/2012. There is also a linear trend in the strength (-0.18 cm yr^{-1}, 5.13% per decade), but the decline in the SPG area ($-3.30 * 10^3$ km^2 yr^{-1}, 1.23% per decade) does not exceed the 95% significant threshold ($p = 0.10$). As seen in Figure 4c, the SSH of the SPG boundary (mean = -34 ± 4 cm) and the SPG center (mean = -68 ± 5 cm) are both increasing over the study period, but the center is increasing more rapidly (0.36 cm yr^{-1}, 5.2% per decade) than the boundary (0.16 cm yr^{-1}, 4.9% per decade), causing the long-term decline in the SPG strength. This result is consistent with the analysis of the Gyre Index indicating that the SPG bowl is flattening and the gyre weakening, but it is occurring at a rate about a quarter of the speed previously published (~5% per decade versus ~20% per decade) [*Häkkinen and Rhines*, 2004]. We note that our SPG metrics are calculated without detrending the SSH data and without removing the seasonal cycle. Due to our definition of the gyre strength as the difference in SSH at the boundary and at the center, variability that exists in both time series is removed by this subtraction.

3.2.3. Comparisons of SPG Strength to In Situ Measurements

To ground-truth our satellite-measured index of the SPG strength (Figure 4b), we compare it to in situ transport and velocity observations of the subpolar North Atlantic. There is strong correspondence between our gyre strength and volume transports of the East Greenland Current calculated along the OVIDE section from 1992 to 2009 using altimetry, OVIDE hydrography and WOCE AR7E sections [*Daniault et al*., 2011]. They measure peaks in 1997, 2002, and 2007 and troughs in 2000 and 2005, which are all consistent with our time series. In addition, the authors find no evidence of a long-term trend in the strength of the East Greenland Current in this reconstruction of the transport. It is worth noting that due to their use of satellite altimetry, this estimate is not entirely independent of our metric.

In addition, *Fischer et al*. [2010] and *Xu et al*. [2013] use a mooring array at 53°N in the Labrador Current to report very little interannual variability in current velocities over the period 1997–2009. On longer time scales, *Fischer et al*. [2010] note that given the accuracy of their observations, linear trends greater than or equal to ~10% of the mean transport should be detected, yet they do not see evidence of such a trend. Extrapolating the trend of the SPG strength calculated here (−5.13% per decade) to the 13 years of their observations yields a 6.67% decline, which is below their detection threshold. In comparison, over the 1997–2009 period, the Gyre Index decreased by 7.6 cm (Figure 2b), or almost 20% of the roughly 40 cm mean SSH slope in the western Labrador Sea (Figure 1a). Such a large change would have been detected by the 53°N array.

In summary, we conclude that our satellite-based index of the barotropic transport is consistent with the in situ transport and velocity measurements—thereby reconciling the variability reported from in situ arrays with the large-scale satellite measurements. However, the long-term trend in the gyre strength that we detect is not evident in the in situ measurements and we posit that a stronger signal is necessary to exceed the thresholds for statistical significance in those studies.

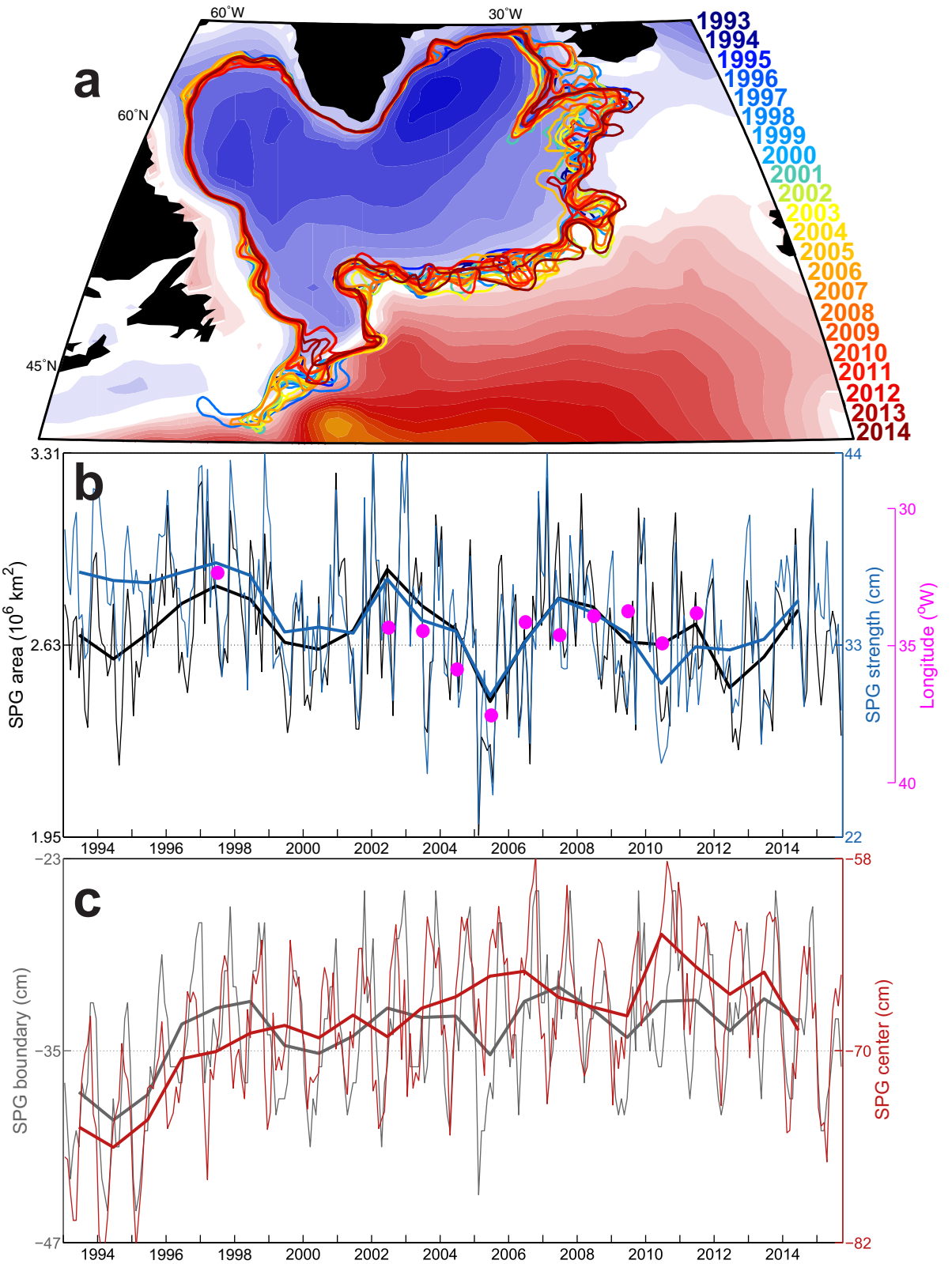

Figure 4. Interannual variability of SPG dilations. (a) SPG boundary in each year from 1993 to 2014. Year names are colored according the color of their boundary. Background colors depict the time-mean stream function from *Rypina et al*. [2011] (color bar same as Figure 3). (b) SPG area (black) and strength (blue) at monthly (thin) and annual time scales (thick). Pink dots refer to the longitude of the subpolar front along a hydrographic section in the Irminger Sea and Iceland Basin at 60°N [*Sarafanov et al*., 2008]. (c) SSH of SPG boundary (gray) and center (red) over the same period. The two *y* axes in **c** are offset by 35 cm but have the same range (24 cm) so that their slopes can be compared. The gyre strength in Figure 4b is calculated as the difference between the two curves in Figure 4c.

3.2.4. Comparisons of SPG Area to In Situ Measurements

We compare our SPG area metric (Figure 4b) to in situ measurements of the gyre's eastern boundary, where, as mentioned above, we expect areal changes to be manifest. The zonal position of the subpolar front (SPF) at 60°N in the Irminger Sea, measured from hydrographic surveys from 1997 to 2011 [*Sarafanov et al*., 2008], provides an independent test of our metric. Based on the location of the 35.0 isohaline at 250 db as the position of the SPF (Figure 4b, pink dots), the SPG is largest in 1997, shrinks dramatically in 2005, rebounds in 2006 and remains relatively steady from 2006 to 2011 [*Sarafanov et al*., 2008] (Sarafanov et al., personal communication, 2016). These changes agree well with our metric of SPG area ($r = 0.70$).

Comparisons of the SPG area with changes in the subpolar property front in the Iceland Basin/Rockall Trough are not as favorable. *Hátún et al*. [2005], *Bersch et al*. [2007], and *Lozier and Stewart* [2008] all use salinity in the eastern SPG to track the longitude of the SPF and none of these time series correlate with our SPG dilations. *Bersch et al*. [2007] report an increase in eastern SPG salinity in 1996/1997 and 2002 and infer that the SPF moved westward in those years. *Lozier and Stewart* [2008] also calculate a westward contraction of the SPF in the late 1990s, and both papers attribute this to a response to the weakened NAO during this time period. *Hátún et al*. [2005] suggest that a switch from a large gyre in 1993 to a smaller gyre in 1998 leads to more Atlantic-to-Arctic exchange of high salinity waters in 1998. Instead, we report a larger gyre in 1997 and 2002.

This agreement between our gyre size and the longitude of the SPF at 60°N [*Sarafanov et al*., 2008] and lack of agreement with the longitude of the SPF at 55°N [*Lozier and Stewart*, 2008] and 53°N [*Bersch et al*., 2007] motivated an analysis of the latitudinal coherence of the eastern SPG boundary (Figure 5). This analysis demonstrates the lack of coherent frontal movements in the SPF—the variability at any one latitude is not representative of the entire eastern SPF. Thus, it is quite likely that the 60°N section from *Sarafanov et al*. [2008], located in the Irminger Sea (38°W–32°W), is summarizing the large variability present in the SPG boundary around the Reykjanes Ridge while the variability in the eastern SPF reported in *Lozier and Stewart* [2008] at 55°N and *Bersch et al*. [2007] at 53°N is capturing a different signal in the eastern Iceland Basin. In fact, if the zonal variability in our gyre boundary at 55°N is considered, the interannual variability of SPG size is only weakly correlated to the SPG area time series ($r = 0.45$) and has a trend toward an eastward expansion of the gyre from 1993 to 2014 of 0.15° longitude per year, in contrast to the decline in both the Gyre Index and the SPG area time series. However, this variability is highly sensitive to the latitude at which one considers due to the large eddy and meandering activity on the eastern boundary (Figure 5c). In addition, the dilations of the SPG are neither connected to the salinity of the eastern SPG (Figure 5d), nor the longitude of the salinity front defined by either a fixed isohaline at a given depth (as in *Sarafanov et al*. [2008] and *Lozier and Stewart* [2008]), or as the maximum zonal gradient in salinity at each time step (not shown). But despite this disconnect, our results (e.g., a large SPG in the late 1990s) do not necessarily contradict previous results on STG throughput variability as measured by salinity in the Rockall Trough (increased STG influence and high salinity in Rockall Trough in the late 1990s). Essentially, we believe it is possible that the property variability in the eastern SPG varies independently (i.e., operating beyond an integral time and/or space scale) of the direct footprint of the SPG dilations—especially given how little our SPG boundary varies in its zonal extent.

3.2.5. Mechanisms of Interannual Variability

Given that positive WSC over the SPG drives the mean SPG strength and structure, we investigate WSC interannual variability as a driver of SPG dilations. An EOF of the winter WSC over the North Atlantic yields two prominent modes that have been previously identified in sea level pressure and geopotential height: the NAO and the EA (Figure 6) [*Comas-Bruand McDermott*, 2014; *Bastos et al*., 2016]. Together these modes account for over 50% of the variability in winter WSC and the percent variance explained by each subsequent mode drops to less than 9% after the second mode. Conceptually, the NAO is a measure of the strength of the westerlies and the EA is a measure of the location or orientation of the westerlies [*Comas-Bru and McDermott*, 2014]. When the EA is positive, the positive WSC that is typically located in the Irminger Sea extends southeastward into the Iceland Basin. Similarly, when the EA is negative, the negative WSC that is typically located over the Azores extends northward into the Iceland Basin. The wintertime correlations between the EA and both the SPG area and strength ($r = 0.51$ for both) indicate that shifts in the WSC centers of action are linked to SPG dilations, albeit weakly. For example, in 2005 when the EA is strongly negative and the NAO is weakly positive, the WSC in the eastern SPG is anomalously negative, yielding a

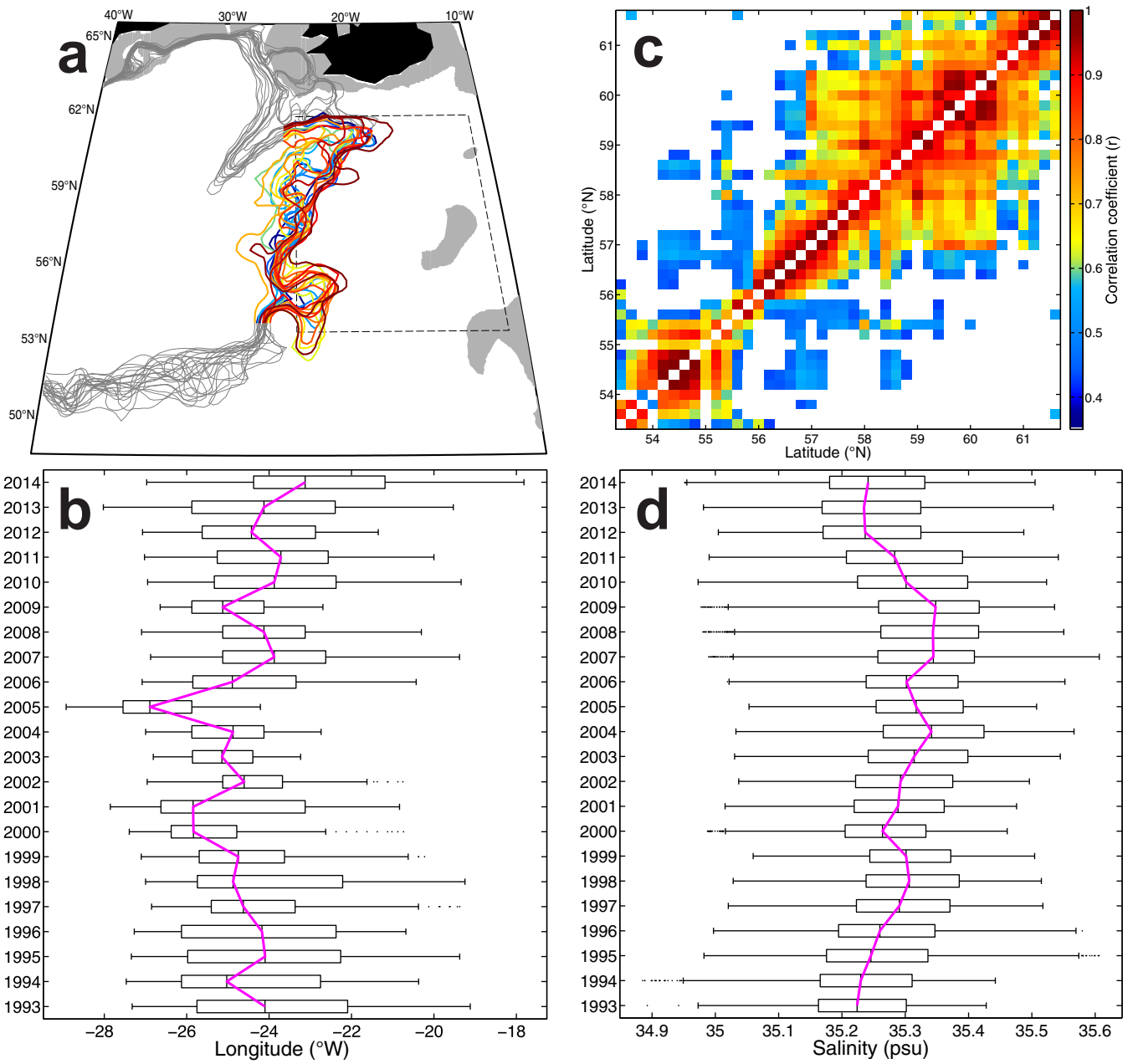

Figure 5. Interannual variability of the SPF. (a) The SPG boundary in each year from 1993 to 2014 with colored portions denoting the region between 53.3°N and 61.6°N where the longitude of the SPF is tracked. (b) Interannual variability in the SPF longitude. The magenta line connects the annual medians, the boxes cover the 50% confidence intervals, and the whiskers cover the 95% confidence interval. The annual median SPF (magenta line) is weakly correlated with the time series of SPG area ($r = 0.45$). (c) Cross correlation of the eastern SPF longitude at each latitude from 53.3°N to 61.6°N. The lack of strong correlations across a wide range of latitudes indicates that the time variability of the eastern SPF at a given latitude is not representative of the entire zonal contraction/expansion of the gyre. All correlations shown are statistically significant ($p < 0.05$). (d) Time variability of salinity in the eastern SPG (black dashed region in Figure 5a; 53°N–62°N, 26°W–10°W, 0–500 m) from the EN4 gridded data set. Neither this time series of the eastern SPG salinity, nor the longitude of the salinity front is correlated to the longitude of the eastern SPF shown in Figure 5b.

collapse in both the size and strength of the SPG despite the positive NAO forcing. This is essentially the same argument that *Häkkinen et al.* [2011] put forth as a mechanism to control the size and strength of the SPG via atmospheric blocking events. However, neither the EA time series that we derive here from the second PC of winter WSC nor the EA time series from the NOAA CPC has a declining trend from 1993 to 2015, further confirmation that the SPG has not been strongly declining over this time period.

A comparison of the linear effect of these two WSC modes on North Atlantic SSH (Figures 7a and 7b) at zero lag reveals that changes in the NAO primarily impact the SSH uniformly over the SPG by raising or

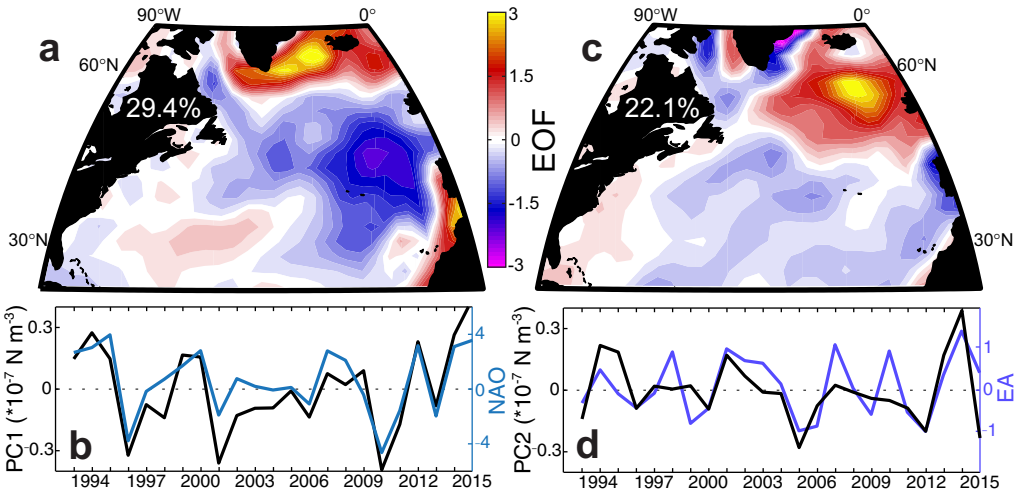

Figure 6. EOF of North Atlantic winter wind stress curl. (a) EOF1 of WSC (29.4% of the variance) depicts the NAO spatial pattern: positive WSC over the Iceland Low and negative WSC over the Azores High. (b) PC1 from 1993 to 2015 is highly correlated ($r = 0.89$) to the winter NAO (blue). (**c**) EOF2 (22.1% of the variance) weights strongly on the region between the Iceland Low and Azores High, effectively controlling the location of the relative centers of action of the NAO. (d) PC2 is correlated ($r = 0.61$) to the winter East Atlantic pattern (purple).

lowering the overall SPG sea level with respect to the STG [*Flatau et al.*, 2003], but NAO changes are not linked to changes in the location or strength of the currents within the SPG. On the other hand, the EA in its positive phase depresses the SSH in the eastern SPG, yielding an expansion in the SPG area.

When the local SSH is regressed onto the time series of SPG area (Figure 7c), the same negative weights emerge in the eastern and southern SPG as in the EA regression (Figure 7b), reinforcing the suggestion that the SSH in the eastern SPG decreases during periods of an expanded SPG. In addition, a positive EA will also displace the central SPG slightly downward with respect to its boundary, deepening the SPG bowl and yielding a stronger gyre. This feature is evident in the regression of local SSH onto the winter SPG strength

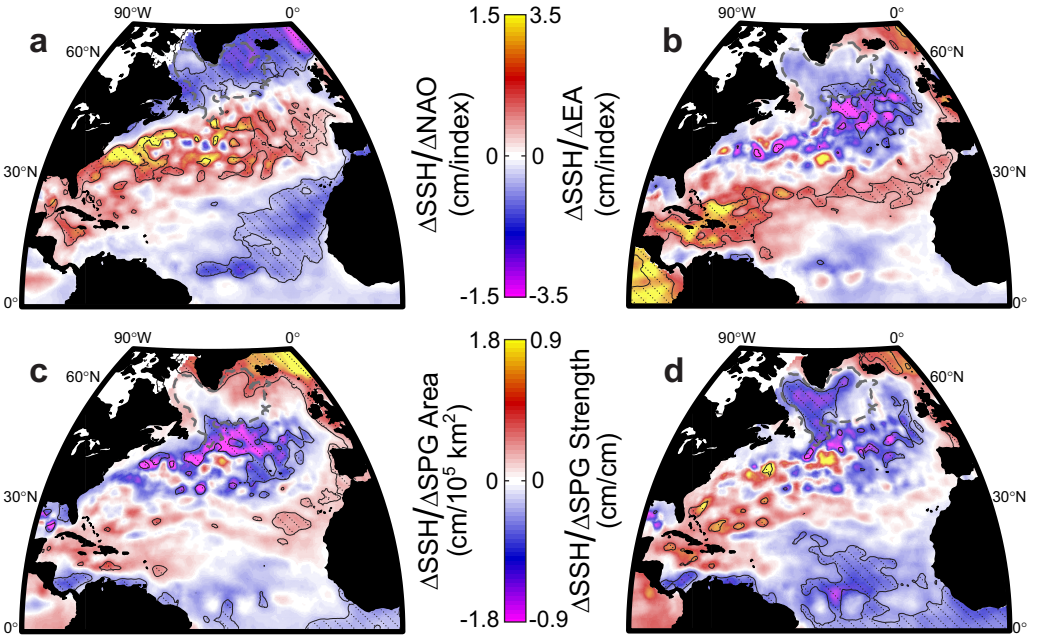

Figure 7. Linear response of North Atlantic SSH to multiple variables. Linear slopes of detrended, winter SSH regressed onto (a) winter NAO, (b) winter EA, (c) winter SPG area, and (d) winter SPG strength. In all plots, the SSH fields were spatially smoothed with a 2.75° × 2.75° median filter prior to calculating the correlations and stippling denotes statistically significant ($p < 0.05$) correlations. The gray dashed line marks the mean SPG boundary.

(Figure 7d), where the SSH in the central Labrador and Irminger Seas decreases when the SPG is strongest, while the SSH of the boundary does not respond. There are also similarities between the SSH regressions on SPG area (Figure 7c) and SPG strength (Figure 7d), particularly in the region just south of the mean SPG boundary. This similarity is expected given that the time series of the two variables are correlated (Figure 4b). Overall, Figure 7 demonstrates that the response of the local SSH to the EA (Figure 7b) is very similar to the changes that coincide with changes in the SPG area (Figure 7c) in the eastern and southern SPG, and has similar patterns to the changes that coincide with changes in the SPG strength (Figure 7d) in the central SPG. Thus, we suggest that the location of the WSC centers of action over the SPG—which is tracked by the EA (Figure 6c)—is impacting the interannual variability of the SPG dilations.

In the past, both the Gyre Index and the NAO have been used to explain variability in the size and strength of the SPG [*Flatau et al.*, 2003; *Häkkinen and Rhines*, 2004; *Bersch et al.*, 2007], but in our EOF analysis the weights for both modes are similar across the SPG (Figures 2a and 2c) and thus their variability correlates to both the gyre center and boundary. For example, the height of the gyre boundary and the height of the gyre center (Figure 4c) both have statistically significant correlations to the NAO when their linear trends are removed. But because both covary with the NAO, the difference between them (i.e., the gyre strength) is not statistically significantly correlated to the NAO. This confirms what we noticed in Figures 2 and 7: the Gyre Index is mainly reflecting the basin-wide displacement of SSH and the NAO is mainly reflecting the relative displacement of the SPG with respect to the STG.

Even though both the Gyre Index and the NAO do weight more negatively in the central SPG regions than the boundary, these are secondary effects and neither index represents a strong signal in the total variability of SPG strength. A mechanism for changing the gyre strength must be able to deepen or flatten the SPG bowl rather than displace the whole SPG bowl up or down. From our analysis, the EA is the most effective at doing that by changing the location of the North Atlantic WSC centers of action that drive the SPG circulation (Figure 7b).

3.3. EOF Analysis of Detrended North Atlantic SSH

We return to an EOF analysis of SSH to determine whether the SPG dilations calculated in section 3.2 are connected to dominant modes of SSH variability. For this EOF, we remove the effect of basin-wide sea level rise on the SSH time series by subtracting the time series of basin-averaged SSH from the local SSH data and normalizing the SSH by the local standard deviation. With this preprocessing, the leading mode (Figures 8a and 8b) represents NAO-induced variability, is nearly identical to the second mode of the initial EOF analysis (Figure 2d) ($r_{monthly} = 0.86$, $r_{annual} = 0.94$), and correlated with the winter NAO time series ($r = 0.73$).

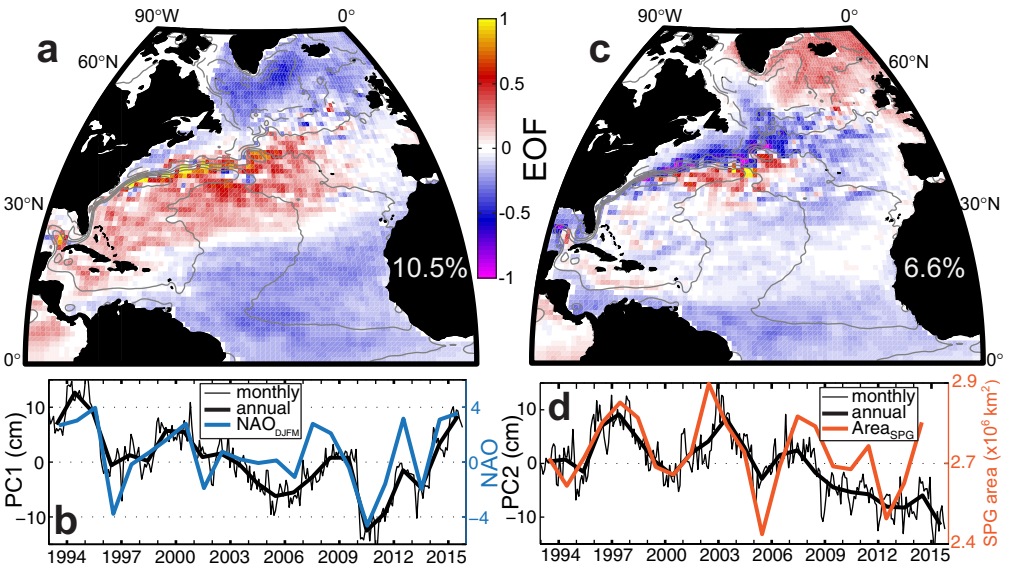

Figure 8. EOF analysis of detrended SSH. (a) EOF1 of detrended North Atlantic SSH (10.5% of the variance) depicts the NAO tripole pattern and (b) PC1 is correlated ($r = 0.73$) to the winter NAO (blue). (c) EOF2 (6.6% of the variance) is similar to the pattern of SSH regressed onto the SPG area (Figure 7c) and (d) PC2 is correlated to the SPG area ($r = 0.63$). Time-mean SSH contours are shown in gray in Figures 7a and 7c (dashed = negative).

Though the normalization is not necessary to recover the NAO tripole pattern, it increases the percent of variance explained from 4.9% to 10.5%. If one only uses the SSH over the SPG (45°N–66°N, 90°W–0°W), the NAO mode explains 25.5% of the variance. We find that by detrending, the Gyre Index mode is removed from the data and the leading mode of variance in the SSH data expresses NAO variability as was reported in *Eden and Esselborn* [2001].

The second mode of the detrended and normalized SSH (Figures 8c and 8d) explains 6.6% (10.0% for SPG-only) of the variance and is related to the SPG dilations as indicated by its correlation to the SPG area ($r_{annual} = 0.63$) and SPG strength ($r_{annual} = 0.58$). The pattern of the spatial weightings appears to be a combination of the linear regressions of local SSH onto SPG area (Figure 7c) and SPG strength (Figure 7d), with strong negative weights along the southeastern edge of the SPG, westward into the Labrador Sea, and southward along the mean GS/NAC position. This implies that when the SPG is large (small) and strong (weak), the SSH in these negative-weighted regions is depressed (elevated), reflecting the expected expansion (contraction) eastward (westward) of the SSH contours and a deepening (flattening) of the SPG bowl. Overall, we find that the second mode of detrended SSH is capturing much of the same variability that the gyre dilations isolate in section 3.2.

4. Conclusions

We use a combination of EOF analysis and direct calculations of the size and strength of the SPG to attribute variability in SPG SSH to three modes: (1) a North Atlantic basin-wide sea level rise, the trend of which is captured by the Gyre Index, (2) the NAO, which produces out-of-phase responses for the SPG and STG, and (3) covarying expansion/contraction and deepening/flattening of the SPG bowl, primarily driven by the location of the winter WSC dipole over the North Atlantic.

From our satellite-derived estimates of the SPG size and strength, we report that the gyre size and strength do indeed covary as was previously assumed, and that oscillations at roughly 5 year time scales dominate the interannual variability in both. These oscillations compare favorably to previous results on SPG dynamics from moorings, hydrography, and satellite altimetry, but do not compare well to salinity variability in the eastern SPG. This mismatch suggests that the size/strength of the SPG does not control the magnitude of STG waters that flow into the eastern SPG, at least on interannual time scales. Combined, these two conclusions—that the NAO is not a dominant control on the size and strength of the SPG and that the SPG size does not influence the strength of the intergyre throughput—leave open the possibility that NAO dynamics control the intergyre throughput, as has been previously suggested [*Curry and McCartney*, 2001; *Bersch*, 2002; *Flatau et al*., 2003; *Lozier and Stewart*, 2008].

Finally, in this work we are able to reconcile a discrepancy between the satellite altimetry and *in situ* estimates of the size and strength of the SPG, the latter of which show no long-term trends. While we do capture a weakening of the gyre strength as had been previously estimated from altimetry [e.g., *Häkkinen and Rhines*, 2004], the size of the gyre is quite stable and the weakening is significantly smaller than previously reported. Both of these results—a slowly weakening gyre and a stable gyre area over the study period—fall within the error bars of the estimates of these variables from in situ observations.

Acknowledgments
We would like to thank Irina Rypina (SPG stream function from surface drifters) and Artem Sarafanov (longitudes of the SPF at 60°N) for providing data for direct comparisons to our results. This work has benefited from discussions with Bill Johns, Sijia Zou, Ryan Peabody, Feili Li, and Femke de Jong. Data used in this analysis are available from the AVISO SSH (https://www.aviso.altimetry.fr/en/data/data-access/aviso-opendap/opendap-adt-products.html), the MetOffice EN4 gridded salinity (http://www.metoffice.gov.uk/hadobs/en4/), the NOAA ESRL wind stresses (https://www.esrl.noaa.gov/psd/data/gridded/data.ncep.reanalysis.derived.surfaceflux.html), the NCAR/UCAR Climate Data Guide NAO (https://climatedataguide.ucar.edu/climate-data/hurrell-north-atlantic-oscillation-nao-index-station-based), and the NOAA CPC EA (http://www.cpc.ncep.noaa.gov/data/teledoc/ea.shtml). This work was funded by a NASA Earth and Space Sciences Graduate Fellowship (NNX13AO21H) and the NSF Physical Oceanography Program (NSF-OCE-12–59102; awarded to MSL). The authors do not report any conflicts of interest.

References

Bastos, A., et al. (2016), European land CO_2 sink influenced by NAO and East-Atlantic Pattern coupling, *Nat. Commun.*, *7*, 10315.
Bersch, M. (2002), North Atlantic Oscillation-induced changes of the upper layer circulation in the northern North Atlantic Ocean, *J. Geophys. Res.*, *107*(C10), 3156, doi:10.1029/2001JC000901.
Bersch, M., I. Yashayaev, and K. P. Koltermann (2007), Recent changes of the thermohaline circulation in the subpolar North Atlantic, *Ocean Dyn.*, *57*, 223–235.
Böning, C. W., M. Scheinert, J. Dengg, A. Biastoch, and A. Funk (2006), Decadal variability of subpolar gyre transport and its reverberation in the North Atlantic overturning, *Geophys. Res. Lett.*, *33*, L21S01, doi:10.1029/2006GL026906.
Cazenave, A., and W. Llovel (2010), Contemporary sea level rise, *Annu. Rev. Mar. Sci.*, *2*, 145–173.
Church, J. A., et al. (2013), Sea level change, in *Climate Change 2013: The Physical Science Basis. Contribution of Working Group I to the Fifth Assessment Report of the Intergovernmental Panel on Climate Change*, edited by T. F. Stocker et al., Cambridge Univ. Press, Cambridge, U. K.
Comas-Bru, L., and F. McDermott (2014), Impacts of the EA and SCA patterns on the European twentieth century NAO-winter climate relationship, *Q. J. R. Meteorol. Soc.*, *140*, 354–363.
Curry, R., and C. Mauritzen (2005), Dilution of the Northern North Atlantic Ocean in recent decades, *Science*, *308*, 1772–1774.

Curry, R., and M. McCartney (2001), Ocean gyre circulation changes associated with the North Atlantic oscillation, *J. Phys. Oceanogr.*, *31*, 3374–3400.
Daniault, N., H. Mercier, and P. Lherminier (2011), The 1992–2009 transport variability of the East Greenland-Irminger Current at 60°N, *Geophys. Res. Lett.*, *38*, L07601, doi:10.1029/2011GL046863.
Deser, C., M. A. Alexander, S. Xie, and A. Phillips (2010), Sea surface temperature variability: Patterns and mechanisms, *Annu. Rev. Mar. Sci.*, *2*, 115–143, doi:10.1146/annurev-marine-120408-151453.
Deshayes, J., and C. Frankignoul (2008), Simulated variability of the circulation in the North Atlantic from 1953 to 2003, *J. Clim.*, *21*, 4919–4933.
Esselborn, S., and C. Eden (2001), Sea surface height changes in the North Atlantic Ocean related to the North Atlantic Oscillation, *Geophys. Res. Lett.*, *28*(18), 3473–3476.
Fischer, J., M. Visbeck, R. Zantopp, and N. Nunes (2010), Interannual to decadal variability of outflow from the Labrador Sea, *Geophys. Res. Lett.*, *37*, L24610, doi:10.1029/2010GL045321.
Flatau, M., L. Talley, and P. Niiler (2003), The North Atlantic oscillation, surface current velocities, and SST changes in the Subpolar North Atlantic, *J. Clim.*, *16*, 2355–2369.
Fratantoni, D. M. (2001), North Atlantic surface circulation during the 1990's observed with satellite-tracked drifters, *J. Geophys. Res.*, *106*(C10), 22,067–22,093.
Good, S. A., M. J. Martin, and N. A. Rayner (2013), EN4: Quality controlled ocean temperature and salinity profiles and monthly objective analysis with uncertainty estimates, *J. Geophys. Res.*, *118*, 6704–6716, doi:10.1002/2013JC009067.
Häkkinen, S., and P. Rhines (2004), Decline of subpolar North Atlantic circulation during the 1990s, *Science*, *304*, 555–559.
Häkkinen, S., and P. Rhines (2009), Shifting surface currents in the northern North Atlantic Ocean, *J. Geophys. Res.*, *114*, C04005, doi:10.1029/2008JC004883.
Häkkinen, S., P. Rhines, and D. Worthen (2011), Atmospheric blocking and Atlantic multidecadal ocean variability, *Science*, *334*, 655–659.
Häkkinen, S., P. Rhines, and D. Worthen (2013), Northern North Atlantic sea surface height and ocean heat content variability, *J. Geophys. Res.*, *118*, 3670–3678, doi:10.1002/jgrc.20268.
Han, G., N. Chen, and Z. Ma (2014), Is there a north-south phase shift in the surface Labrador Current transport on the interannual-to-decadal scale?, *J. Geophys. Res.*, *119*, 276–287, doi:10.1002/2013JC009102.
Han, G., K. Ohashi, N. Chen, P. G. Myers, N. Nunes, and J. Fisher (2010), Decline and partial rebound of the Labrador Current 1993–2004: Monitoring ocean currents from altimetric and conductivity-temperature-depth data, *J. Geophys. Res.*, *115*, C12012, doi:10.1029/2009JC006091.
Hátún, H., A. B. Sandø, H. Drange, B. Hansen, and H. Valdimarsson (2005), Influence of the Atlantic subpolar gyre on the thermohaline circulation, *Science*, *309*, 1841–1844.
Holliday, P. (2003), Air-sea interaction and circulation changes in the northeast Atlantic, *J. Geophys. Res.*, *108*(C8), 3259, doi:10.1029/2002JC001344.
Hurrell, J., and National Center for Atmospheric Research Staff (Eds.), The Climate Data Guide: Hurrell North Atlantic Oscillation (NAO) Index (station-based), Last modified 13 May 2016. [Retrieved from https://climatedataguide.ucar.edu/climate-data/hurrell-north-atlantic-oscillation-nao-index-station-based.]
Johnson, C., M. Inall, and S. Häkkinen (2013), Declining nutrient concentrations in the northeast Atlantic as a result of a weakening Subpolar Gyre, *Deep Sea Res., Part I*, *82*, 95–107.
Kalnay, E., et al., (1996), The NCEP/NCAR 40-year reanalysis project, *Bull. Am. Meteorol. Soc.*, *77*, 437–470.
Lavender, K., R. E. Davis, and W. B. Owens (2005), Mid-depth recirculation observed in the interior Labrador and Irminger seas by direct velocity measurements, *Nature*, *407*, 66–69.
Lozier, M. S., and N. M. Stewart (2008), On the temporally varying northward penetration of Mediterranean Overflow Water and eastward penetration of Labrador Sea Water, *J. Phys. Oceanogr.*, *38*, 2097–2103.
Lozier, M. S., S. Leadbetter, R. G. Williams, V. Roussenov, M. S. C. Reed, and N. J. Moore (2008), The spatial pattern and mechanisms of heat-content change in the North Atlantic, *Science*, *319*, 800–803.
Manly, B. F. J. (2005), *Multivariate Statistical Methods: A Primer*, 3rd ed., Chapman and Hall, London.
Marshall, J., H. Johnson, and J. Goodman (2001), The interaction of the North Atlantic Oscillation with ocean circulation, *J. Clim.*, *14*, 1399–1421.
Palter, J. B., C.-A. Caron, K. Lavender-Law, J. Willis, D. S. Trossman, I. Yashayaev, and D. Gilbert (2016), Variability of the directly observed, middepth subpolar North Atlantic circulation, *Geophys. Res. Lett.*, *43*, 2700–2708, doi:10.1002/2015GL067235.
Perez-Hernandez, M. D., and T. M. Joyce (2014), Two modes of Gulf Stream variability revealed in the last two decades of satellite altimeter data, *J. Phys. Oceanogr.*, *44*, 149–163.
Rossby, T. (1996), The North Atlantic Current and Surrounding Waters: At the crossroads, *Rev. Geophys.*, *34*(4), 463–481.
Rypina, I., L. J. Pratt, and S. Lozier (2011), Near-surface transport pathways in the North Atlantic Ocean: Looking for throughput from the subtropical to the subpolar gyre, *J. Phys. Oceanogr.*, *41*, 911–925.
Sarafanov, A., A. Falina, A. Sokov, and A. Demidov (2008), Intense warming and salinification of intermediate waters of southern origin in the eastern subpolar North Atlantic in the 1990s to mid-2000s, *J. Geophys. Res.*, *113*, C12022, doi:10.1029/2008JC004975.
Sarafanov, A., A. Falina, H. Mercier, A. Sokov, P. Lherminier, C. Gourcuff, S. Gladyshev, F. Gaillard, and N. Daniault (2012), Mean full-depth summer circulation and transports at the northern periphery of the Atlantic Ocean in the 2000s, *J. Geophys. Res.*, *117*, C01014, doi:10.1029/2011JC007572.
Sherwin, T. J., J. F. Read, N. P. Holliday, and C. Johnson (2012), The impact of changes in North Atlantic Gyre distribution on water mass characteristics in the Rockall Trough, *ICES J. Mar. Sci.*, *69*(5), 751–757.
Williams, R. G., V. Roussenov, D. Smith, and M. S. Lozier (2014), Decadal evolution of ocean thermal anomalies in the North Atlantic: The effects of Ekman, overturning and horizontal transport, *J. Clim.*, *27*, 698–719.
Xu, X., H. E. Hurlburt, W. J. Schmitz, R. Zantopp, J. Fischer, and P. J. Hogan (2013), On the currents and transports connected with the Atlantic meridional overturning circulation in the subpolar North Atlantic, *J. Geophys. Res.*, *118*, 502–516, doi:10.1002/jgrc.20065.
Zantopp, R., J. Fisher, M. Visbeck, and J. Karstensen (2017), From interannual to decadal: 17 years of boundary current transports at the exit of the Labrador Sea, *J. Geophys. Res.*, *122*, 1724–1748, doi:10.1002/2016JC012271.
Zhang, R. (2008), Coherent surface-subsurface fingerprint of the Atlantic meridional overturning circulation, *Geophys. Res. Lett.*, *35*, L20705, doi:10.1029/2008GL035463.